Linear Instability of Turbulent Channel Flow

Pavan V. Kashyap,[1,2] Yohann Duguet,[1] and Olivier Dauchot[3]
[1]LIMSI-CNRS, UPR 3251, Université Paris-Saclay, 91405 Orsay, France
[2]Department of Mechanical Engineering, Indian Institute of Science, Bengaluru 560012, India
[3]Gulliver Lab, UMR CNRS 7083, ESPCI Paris, PSL University, 75005 Paris, France

(Received 12 May 2022; revised 3 September 2022; accepted 14 November 2022; published 9 December 2022)

Laminar-turbulent pattern formation is a distinctive feature of the intermittency regime in subcritical plane shear flows. By performing extensive numerical simulations of the plane channel flow, we show that the pattern emerges from a spatial modulation of the turbulent flow, due to a linear instability. We sample over many realizations the linear response of the fluctuating turbulent field to a temporal impulse, in the regime where the turbulent flow is stable, just before the onset of the instability. The dispersion relation is constructed from the ensemble-averaged relaxation rates. As the instability threshold is approached, the relaxation rate of the least damped modes eventually reaches zero. The method allows, despite the presence of turbulent fluctuations and without any closure model, for an accurate estimation of the wave vector of the modulation at onset.

DOI: 10.1103/PhysRevLett.129.244501

Turbulent channel flow is one of the most studied prototypes of inhomogeneous anisotropic turbulence. It has been evidenced, both experimentally and numerically, that at moderate flow rates—quantified by the Reynolds number Re—it exhibits a spatiotemporally intermittent regime featuring robust large-scale turbulent structures amid a laminar background [1–3]. The dynamical origin of such patterned turbulence in channel flow, as well as in other shear flows, remains however actively debated [4–15].

On the lower end in Re of the coexistence regime, turbulent patches grow and split, or decay, resulting in strongly fluctuating dynamics. It was suggested that the stochastic nature of these processes, which decides whether turbulence will either spread or recede and eventually decay, could be described in the framework of nonequilibrium critical phenomena and specifically of directed percolation (DP), with the laminar state acting as the absorbing phase [16]. A major achievement of the past two decades has been to provide strong experimental and numerical evidence in favor of this scenario in a few shear flows [14,17,18]. On the theoretical side, this regime has been described by an effective one-dimensional model of fronts in an excitable medium [19,20]. Quite remarkably, and yet not theoretically understood, numerical simulations of the stochastic version of that model reproduce the DP scenario.

Increasing Re, individual turbulent patches leave place to a well organized periodic pattern of alternating laminar and turbulent bands, inclined at a well-defined angle to the mean flow [4–6]. Considering the proliferation of turbulence as a problem of front propagation, it is tempting to view this pattern as packed arrays of individual localized structures. Yet, periodic pattern solutions have not been identified as solutions to the effective excitable dynamics [19,20]. An alternative viewpoint is to consider the pattern as emerging from the featureless turbulence found at larger Re. Pioneering studies have demonstrated experimentally that the pattern developing in plane and circular Couette flows, characterized by two competing orientations of alternate sign, is fully captured by the dynamics of two coupled Ginburg-Landau equations with noise [6,7]. Recent visualizations, obtained in well-resolved numerical simulations of large domain channel flows, unveil small-amplitude harmonic modulations of the turbulent flow for values of Re larger than those at which genuine laminar-turbulent coexistence is reported [3]. Statistical signatures of low-wall-shear-rate intermittency have been found, at Re-values usually associated with featureless turbulent flows [21]. Altogether these results suggest the possibility of a large-wavelength instability of the *turbulent flow* itself, as already proposed in Ref. [6]. As recently suggested on the basis of a spatiotemporal extension of a classical self-sustained turbulence model [22,23], the instability could be of Turing type [10]. However, there is no theoretical evidence for such a linear instability of the turbulent mean flow obtained from one-point closure models [24]. These different viewpoints reflect global doubts regarding the origins of the patterned state and ambiguity as to whether the starting point for modeling the periodic pattern should be the spatial organization of the isolated turbulent patches when increasing Re, or the linear instability of the turbulent flow, including its fluctuations, when decreasing Re.

Here we bring direct evidence in favor of the linear instability scenario in the case of the channel flow. To do so, we perform extensive numerical simulations and sample the linear response of the turbulent flow to a temporal impulse, in the regime where the large wavelength modulations are damped. The dispersion relation is then constructed from the ensemble-averaged relaxation rates, for decreasing values of Re. The smallest relaxation rate approaches zero for some critical value Re_c, pointing at the spatial structure of the modes which grow at the instability onset. The method can be seen as the temporal counterpart of the spatial linear response considered in Ref. [25]. It is intrinsically statistical in the sense that it establishes an *average dispersion relation* for the instability modes, from which the quantitative onset for the spatial modulation can be identified.

The incompressible flow considered in this study is driven in the streamwise direction x by a constant pressure gradient. The other Cartesian coordinates y and z are respectively wall normal and spanwise. All length scales are nondimensionalized by the channel half gap h, and velocities $\mathbf{u} = (u_x, u_y, u_z)$ by U_{cl}, the centerline velocity of the classical laminar plane Poiseuille flow $U(y) = 1 - y^2$ driven by the same pressure gradient. Time is reported in units of h/U_{cl}. The velocity field is decomposed as $\mathbf{u} = U(y)\mathbf{e}_x + \mathbf{u}'$ where $\mathbf{u}'$ denotes the perturbation to the laminar base flow. Spatial average of a field f are indicated with $\langle f \rangle_{x,y,z}$ where the subscript indicates the direction over which the average is computed. Time averages are indicated by $\bar{f}$. Ensemble averages are indicated as $\langle f \rangle_e$. Fourier amplitudes are denoted with $\hat{f}$. The selected control parameter is the friction Reynolds number $\mathrm{Re}_\tau = u_\tau h/\nu$, where ν is the kinematic viscosity of the fluid, $u_\tau = \sqrt{\langle \bar{\tau} \rangle_{xz}/\rho}$ is the friction velocity, with $\langle \bar{\tau} \rangle_{xz}$ the mean shear rate fixed by the pressure gradient, and ρ the fluid density. Turbulent simulations were performed with the spectral solver CHANNELFLOW2.0 [26] in a domain of $L_x = 2L_z = 250$ for times up to $t = 4000$. These simulations are resolved with a resolution of $N_x = N_z = 1024$ (including dealiasing with the 2/3 rule) and $N_y = 65$ comparable to Ref. [3]. The most recent investigations have reported laminar-turbulent patterns for $50 \lesssim \mathrm{Re}_\tau \lesssim 90$, and independent turbulent bands for lower values of Re_τ down to ≈ 36 [3,21,27,28].

Large-scale modulations close to $\mathrm{Re}_\tau \approx 90$, as well as genuine laminar-turbulent patterning for $\mathrm{Re}_\tau \lesssim 90$, are unambiguous from Fig. 1, which displays the instantaneous kinetic energy in the wall-normal direction

$$E_v(x, z, t) = \left\langle \frac{1}{2} u_y'^2 \right\rangle_y, \tag{1}$$

both at full spatial resolution and after application of a low-pass filter. It was checked that the modulations and the pattern are robust with respect to the doubling and quadrupling of the numerical domain in both x and z (see Appendix A of the Supplemental Material [29]). The exact

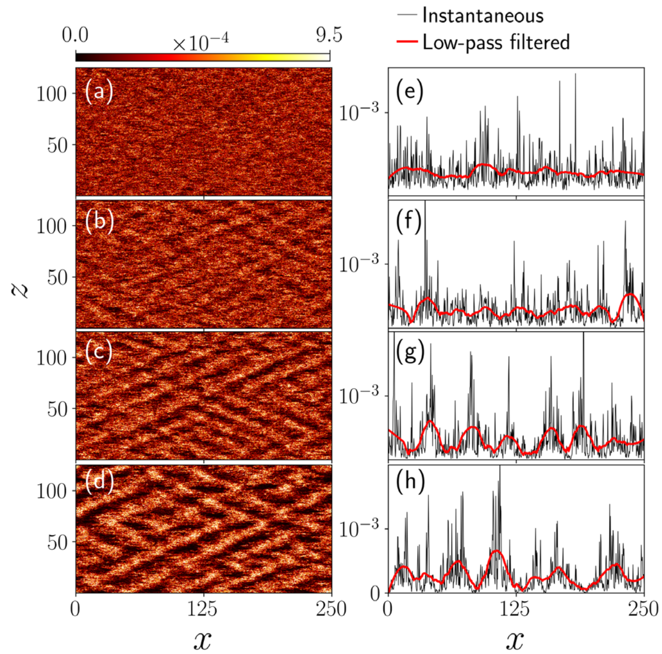

FIG. 1. Onset of modulated turbulent channel flow. Left column: turbulent kinetic energy $E_v(x, z, t)$. Right column: instantaneous streamwise profile of $E_v(x, z = cst, t)$, (black: raw instantaneous values; red: low-pass filtered values). From top to bottom: (a), (e) $\mathrm{Re}_\tau = 100$, (b), (f) $\mathrm{Re}_\tau = 90$, (c), (g) $\mathrm{Re}_\tau = 85$, (d), (h) $\mathrm{Re}_\tau = 80$.

range of existence of the modulations, and notably their onset, are difficult to judge from visualizations alone because of the turbulent fluctuations, whose standard deviation can exceed the amplitude of the modulation. It is also sensitive to the choice of the visualized quantity. Conversely, the emergence of large-scale patterns, as Re_τ decreases, appears clearly as a low-wave-number signature in the time-averaged two-dimensional energy spectrum of the y-averaged fluctuating streamwise component $\langle u_x' \rangle_y$ [Fig. 2(a)]. Apart from the small-scale modes, corresponding to the turbulent fluctuations, one clearly observes a set of large-scale modes excited at $\mathrm{Re}_\tau = 92$ (but absent at $\mathrm{Re}_\tau = 110$). We also note an increase of the energy contained in the small-scale modes, and in the modes separating them from the large-scale ones, as Re_τ decreases. The detailed mechanisms of such energy transfer in the spectral space have been analyzed recently in turbulent shear flows at a low [30], moderate [31], and high [32] Reynolds number. They rely on the combined nonlinear action of direct, inverse, and especially transverse cascades [33], in contrast to the classical cascade picture. Our contribution deals with the cause for the *sudden* strengthening-activation (upon lowering Re) of these energy transfers toward large scales and to the methodology for identifying the associated critical threshold in Re.

Two maxima are readily identified in Fig. 2(a). Exploiting this scale separation, we define $\mathcal{E}_{\mathrm{LSF}}(\mathrm{Re}_\tau)$,

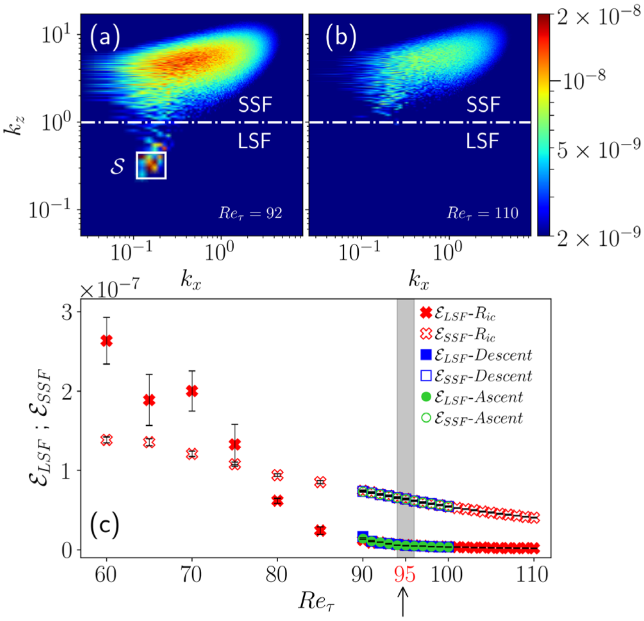

FIG. 2. Premultiplied power spectrum for the y-averaged streamwise velocity fluctuation $\langle u_x' \rangle_y$ at (a) $\mathrm{Re}_\tau = 92$ and (b) $\mathrm{Re}_\tau = 110$ (right). (c) Energies $\mathcal{E}_{\mathrm{LSF}}$ of the large-scale modes (defined according to Eq. (2) and $\mathcal{E}_{\mathrm{SSF}}$ of the small-scale modes vs Re_τ. The black arrow points at the linear instability threshold corresponding to the onset of the turbulent modulated flow determined here at $\mathrm{Re}_\tau = 95 \pm 1$. $\mathcal{E}_{\mathrm{LSF}}$ (filled symbols) and $\mathcal{E}_{\mathrm{SSF}}$ (empty symbols) are computed for different simulation strategies: red cross, R_{IC}, divergence free random velocity field as initial condition; blue square, descending annealing; green circle, ascending annealing.

and $\mathcal{E}_{\mathrm{SSF}}(\mathrm{Re}_\tau)$, the dimensionless amplitude of the large-scale and small-scale flows, as the energy content of the spectral subdomains $\mathcal{S}_{\mathrm{LSF}} = \{0 < k_z < 1\}$ and $\mathcal{S}_{\mathrm{SSF}} = \{1 \lesssim k_z\}$, respectively:

$$\mathcal{E}_{\mathrm{LSF/SSF}}(\mathrm{Re}_\tau) = \iint_{\mathcal{S}_{\mathrm{LSF/SSF}}} |\langle \bar{\hat{u}}_x' \rangle_y|^2 dk_x dk_z. \qquad (2)$$

$\mathcal{E}_{\mathrm{LSF}}$ is dominated by the low-k modes inside the spectral subdomain $\mathcal{S}$ highlighted in Fig. 2(a) (left). We checked that this scale separation, based solely on k_z, appropriately delineates the two energy peaks observed in the spectra of all the turbulent fields we analyzed. $\mathcal{E}_{\mathrm{LSF}}$ and $\mathcal{E}_{\mathrm{SSF}}$ are shown as functions of Re_τ in Fig. 2(c) obtained from random initial conditions (R_{IC}) or during slow ascent, respectively descent, annealing in Re_τ. One observes a clear increase of $\mathcal{E}_{\mathrm{LSF}}$ in contrast with the marginal increase of $\mathcal{E}_{\mathrm{SSF}}$ as Re_τ decreases from the featureless turbulent regime ($\mathrm{Re}_\tau \gtrsim 110$) to the well-defined pattern one ($50 \lesssim \mathrm{Re}_\tau \lesssim 90$), with no sign of hysteresis. We note that $\mathcal{E}_{\mathrm{LSF}}$ is never strictly zero even at high Re_τ. Whether the above observations result from a true bifurcation or are simply a mere crossover cannot be decided by simply looking at Fig. 2. This is what motivates the following analysis where we show that the rise of $\mathcal{E}_{\mathrm{LSF}}$ is due to a linear instability of the turbulent flow.

Establishing the linear instability of a flow with arbitrary time dependence can be addressed in different ways. One possibility is to study the linear stability of the *mean* flow using the Orr-Sommerfeld formalism. This strategy, whether conducted at high [34] or transitional [35] Re, predicts linear stability. At the opposite end, taking into account all temporal fluctuations is in principle possible using Lyapunov analysis. However for turbulent flows the number of positive Lyapunov exponents is prohibitively huge [36] because of the chaoticity at small scales down to the Kolmogorov scale. The turbulent scales where these instabilities dominate are however *not* the emerging large scales visible in Fig. 2, which suggests the computation of alternative quantities.

The general idea is to study the linear response of the flow to a temporal impulse. If the flow is linearly stable, the disturbance should relax; otherwise it should grow and lead to a bifurcated flow. However, the reference flow being turbulent, the analysis must be conducted at a statistical level. Besides the spatial structure of the temporal impulse should be agnostic to the turbulent spectrum. We therefore proceed as follows. A representative turbulent state in the statistically steady regime at the required value of Re_τ, simulated for $t < 0$, is perturbed at $t = 0$ using a divergence-free *noise field*, before the simulations run further without noise, for $t > 0$, and we monitor the temporal evolution of the modulus of the Fourier amplitudes of *large-scale modes*, $|\hat{\tau}|(\mathrm{Re}_\tau, k_x, k_z, t)$, with $(k_x, k_z) \in \mathcal{S} = \{0.075 \lesssim k_x \lesssim 0.22, 0.2 \lesssim k_z \lesssim 0.5\}$ [the highlighted square area in Fig. 2(a), part of $\mathcal{S}_{\mathrm{LSF}}$]. For large enough Re_τ, the disturbed flow relaxes back toward the steady turbulent state. The individual time series $|\hat{\tau}|$ however showcase a strongly fluctuating decay. This computational decay experiment is therefore repeated over 40 different realizations of the noise field and the modulus of the spectral amplitude of each large-scale Fourier mode $|\hat{\tau}|$ is ensemble averaged over all realizations to yield $\langle|\hat{\tau}|\rangle_e$, as illustrated in Fig. 3(a) for $\mathrm{Re}_\tau = 120$ and $(k_x, k_z) = (0.12, 0.3)$. Ensemble averaging brings clarity into the system's response: past an initially nonlinear decrease of $\langle|\hat{\tau}|\rangle_e$, a clear exponential decay toward a finite value A_s is observed. This late stage exponential decay captures the *averaged linear response* of the turbulent state with respect to a temporal impulse, and as such does not depend on the amplitude of the initial noise field. It is our central object of interest, as it gives access to the dispersion relation. The corresponding growth rate σ is evaluated by estimating first the saturation level A_s and then fitting an exponential decay to $(\langle|\hat{\tau}|\rangle_e - A_s)$, using a straight line fit in logarithmic scale, as portrayed in Fig. 3(b) (See Appendix B of the Supplemental Material [29] for a detailed step by step description of the procedure). As a first step, the analysis is

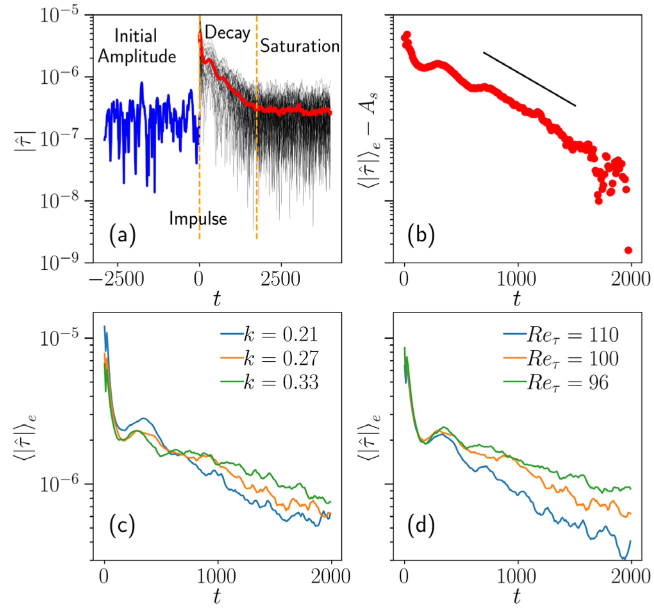

FIG. 3. (a) Temporal evolution of the amplitude of the Fourier mode $|\hat{\tau}|(\mathrm{Re}_\tau, k_x, k_z, t)$ with $(k_x, k_z) = (0.12, 0.3)$, $(k = 0.32)$ and $\mathrm{Re}_\tau = 120$; blue $(t < 0)$; black, individual realizations for $t > 0$; and red, ensemble average $\langle|\hat{\tau}|\rangle_e(t)$. (b) $\langle|\hat{\tau}|\rangle_e(t) - A_s$, same (k_x, k_z), same Re_τ; black, exponential fit. (c) $\langle|\hat{\tau}|\rangle_e(t)$ for three different values of k, $\mathrm{Re}_\tau = 100$. (d) $\langle|\hat{\tau}|\rangle_e(t)$ for three different values of Re_τ, $k = 0.27$.

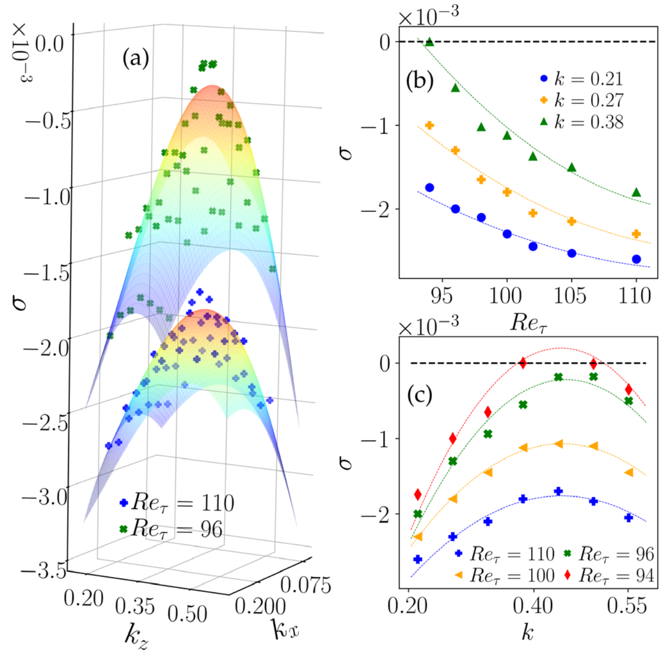

FIG. 4. Dispersion relation. (a) Growth rate σ versus both k_x and k_z for two values of $\mathrm{Re}_\tau = 96$ and 110. (b) Growth rate σ versus Re_τ parametrized by the wave number modulus $k = \sqrt{k_x^2 + k_z^2}$. (c) Growth rate σ versus the wave number modulus k parametrized by Re_τ [The data in (a) is fitted with a paraboloid surface while in (b) and (c) the continuous curves are guides to the eye].

carried out along the diagonal of the spectral window $\mathcal{S}$. Figures 3(c) and 3(d) show the strong dependence of the growth rate on both $k = \sqrt{k_x^2 + k_z^2}$ and Re_τ. More specifically, one observes that, for $\mathrm{Re}_\tau = 96$, the growth rate of the mode corresponding to $k = 0.38$ is close to vanishing, suggesting the proximity of a linear instability. In principle one could expect monitoring the average exponential growth of such a large-scale mode beyond the instability threshold. However, not only would the growth rate be hard to measure accurately near onset, one would also need to isolate the featureless turbulent state in a regime where it is unstable.

We therefore concentrate on the decay rates and extract the mean dispersion relation for the linear response of the turbulent flow (Fig. 4). The data are fit with a paraboloid surface [Fig. 4(a)] of the form

$$\sigma = \alpha(k_x - k_{xc})^2 + \beta(k_z - k_{zc})^2 + \gamma(k_x - k_{xc})(k_z - k_{zc}) + \delta, \tag{3}$$

where (k_{xc}, k_{zc}) is the critical wave vector. The coefficients of Eq. (3) obtained for different values of Re_τ are reported in the Supplemental Material [29], Appendix B. The dispersion curves approach the neutral axis as the value of Re_τ is decreased and eventually cross it for $\mathrm{Re}_\tau = 94$. The estimated critical value for the instability is $\mathrm{Re}_\tau = 95 \pm 1$. The critical wave vector $(k_{xc} = 0.18 \pm 0.025, k_{zc} = 0.42 \pm 0.05)$ is obtained from the above parabolic fit of the decay rates, estimated for all $(k_x, k_z) \in \mathcal{S}$, as illustrated in Fig. 4(a) for $\mathrm{Re}_\tau = 110$ and $\mathrm{Re}_\tau = 96$. It perfectly matches the one measured directly at onset and leads to an inclination of the pattern with the streamwise direction of $23 \pm 0.5°$, consistently with the measurements reported in Ref. [21]. This quantitative agreement validates the proposed methodology, i.e., the statistical analysis of the temporal impulse response can be considered as a new experimental-numerical method to address the linear stability analysis of a steady, but fluctuating dynamics. We emphasize again that the base flow for the analysis is the turbulent flow itself, including all fluctuations [37], not the mean flow.

Altogether our results provide direct evidence for a linear instability of the turbulent state itself, as first conjectured in Ref. [6]. This linear instability leads to a spatial modulation of the turbulent flow, the amplitude of which grows and saturates according to weakly nonlinear contributions [7]. For low enough Re_τ, the modulation breaks into a pattern of alternated turbulent and laminar bands. Further decreasing Re_τ these bands gain in independence, and a proper stochastic front dynamics sets in.

Our Letter paves the way for future works in two main directions. First, one would like to identify the instability mechanism. A possible candidate, commonly encountered across diverse noisy chemical and biological systems [38] relies on the Turing instability [10,39]. It is based on the competition between an inhibitor and an activator field with different diffusivities [40]. However this approach requires modeling of the turbulent diffusivity using, e.g., simple first-moment closures [41,42]. Another possible approach is to consider a generalized stability analysis taking into account higher-order moments of the fluctuations [43]. Both approaches are based on closure assumptions. The instability unveiled in the present Letter represents an ideal and simple case to test these assumptions. The second future direction of research consists in identifying the strongly nonlinear scenario along which the pattern loses its spatial coherence. It remains a formidable challenge.

This study was made possible using computational resources from IDRIS (Institut du Développement et des Ressources en Informatique Scientifique) and the support of its staff. The developing team of channelflow.ch is also gratefully thanked. The authors also acknowledge constructive discussions with D. Barkley, L. S. Tuckerman, S. Gomé, and P. Manneville.

[1] T. Tsukahara, Y. Seki, H. Kawamura, and D. Tochio, *Fourth International Symposium on Turbulence and Shear Flow Phenomena* (Begel House Inc., 2005).
[2] S. Hashimoto, A. Hasobe, T. Tsukahara, Y. Kawaguchi, and H. Kawamura, in *Turbulence Heat and Mass Transfer 6. Proceedings of the Sixth International Symposium On Turbulence Heat and Mass Transfer* (Begel House Inc., Rome, 2009).
[3] M. Shimizu and P. Manneville, Phys. Rev. Fluids **4**, 113903 (2019).
[4] D. Coles, J. Fluid Mech. **21**, 385 (1965).
[5] C. V. Atta, J. Fluid Mech. **25**, 495 (1966).
[6] A. Prigent, G. Grégoire, H. Chaté, O. Dauchot, and W. van Saarloos, Phys. Rev. Lett. **89**, 014501 (2002).
[7] A. Prigent, G. Grégoire, H. Chaté, and O. Dauchot, Physica (Amsterdam) **174D**, 100 (2003).
[8] Y. Duguet, P. Schlatter, and D. S. Henningson, J. Fluid Mech. **650**, 119 (2010).
[9] D. Samanta, A. De Lozar, and B. Hof, J. Fluid Mech. **681**, 193 (2011).
[10] P. Manneville, Europhys. Lett. **98**, 64001 (2012).
[11] P. Manneville and M. Shimizu, arXiv:1904.03739.
[12] C. S. Paranjape, Y. Duguet, and B. Hof, J. Fluid Mech. **897** (2020), 10.1017/jfm.2020.322.
[13] C. Liu and D. F. Gayme, J. Fluid Mech. **927** (2021). 10.1017/jfm.2021.762
[14] L. Klotz, G. Lemoult, K. Avila, and B. Hof, Phys. Rev. Lett. **128**, 014502 (2022).
[15] K. Kohyama, M. Sano, and T. Tsukahara, Phys. Fluids **34**, 084112 (2022).
[16] Y. Pomeau, Physica (Amsterdam) **23D**, 3 (1986).
[17] G. Lemoult, L. Shi, K. Avila, S. V. Jalikop, M. Avila, and B. Hof, Nat. Phys. **12**, 254 (2016).
[18] M. Chantry, L. S. Tuckerman, and D. Barkley, J. Fluid Mech. **824**, R1 (2017).
[19] D. Barkley, Phys. Rev. E **84**, 016309 (2011).
[20] D. Barkley, J. Phys. **318**, 032001 (2011).
[21] P. V. Kashyap, Y. Duguet, and O. Dauchot, Entropy **22**, 1001 (2020).
[22] F. Waleffe, Phys. Fluids **9**, 883 (1997).
[23] O. Dauchot and N. Vioujard, Eur. Phys. J. B **14**, 377 (2000).
[24] L. S. Tuckerman, D. Barkley, and O. Dauchot, in *Seventh IUTAM Symposium on Laminar-Turbulent Transition* (Springer Netherlands, Dordrecht, 2010), Vol. 18, pp. 59–66, ISBN 978-90-481-3722-0, 978-90-481-3723-7.
[25] S. Russo and P. Luchini, J. Fluid Mech. **790**, 104 (2016).
[26] J. Gibson, F. Reetz, S. Azimi, A. Ferraro, T. Kreilos, H. Schrobsdorff, N. Farano, A. F. Yesil, S. S. Schütz, M. Culpo *et al.*, https://www.channelflow.ch/.
[27] B. Song and X. Xiao, J. Fluid Mech. **903** (2020), 10.1017/jfm.2020.636.
[28] V. Mukund, C. Paranjape, M. P. Sitte, and B. Hof, arXiv:2112.06537.
[29] See Supplemental Material at http://link.aps.org/supplemental/10.1103/PhysRevLett.129.244501 for specific informations about the simulations and statistics.
[30] S. Gomé, Ph.D. thesis, Sorbonne Université Paris-Saclay, 2022.
[31] S. Symon, S. J. Illingworth, and I. Marusic, J. Fluid Mech. **911** (2021). 10.1017/jfm.2020.929
[32] M. Lee and R. D. Moser, J. Fluid Mech. **860**, 886 (2019).
[33] G. Mamatsashvili, G. Khujadze, G. Chagelishvili, S. Dong, J. Jiménez, and H. Foysi, Phys. Rev. E **94**, 023111 (2016).
[34] W. Reynolds and W. Tiederman, J. Fluid Mech. **27**, 253 (1967).
[35] L. S. Tuckerman, D. Barkley, and O. Dauchot (private communication).
[36] L. Keefe, P. Moin, and J. Kim, J. Fluid Mech. **242**, 1 (1992).
[37] A. S. Iyer, F. D. Witherden, S. I. Chernyshenko, and P. E. Vincent, J. Fluid Mech. **875**, 758 (2019).
[38] M. Cross and H. Greenside, *Pattern Formation and Dynamics in Nonequilibrium* (Cambridge University Press, Cambridge, England, 2009), ISBN 978-0-521-77050-7.
[39] P. Kashyap, Ph.D. thesis, Université Paris-Saclay, 2021.
[40] A. M. Turing, Phil. Trans. R. Soc. B **237**, 37 (1952).
[41] W. Reynolds and A. Hussain, J. Fluid Mech. **54**, 263 (1972).
[42] J. C. Del Alamo and J. Jimenez, J. Fluid Mech. **559**, 205 (2006).
[43] V. K. Markeviciute and R. R. Kerswell, arXiv:2201.01540.